A new perspective on the impacts of *Spartina alterniflora* invasion on Chinese wetlands in the context of climate change: a case study of the Jiuduansha Shoals, Yangtze Estuary

Min Zhang[1], Christian Schwarz[2,3], Wenpeng Lin[1*], Htun Naing[4], Huayang Cai[5], Zhenchang Zhu[6]

[1] School of Environmental and Geographical Sciences, Shanghai Normal University, Shanghai 200234, China

[2] Department of Civil Engineering, KU Leuven, Leuven, Belgium

[3] Department of Earth and Environmental Sciences, KU Leuven, Leuven, Belgium

[4] Blue Carbon Research Department, Worldview International Foundation, Yangon, Myanmar

[5] School of Marine Engineering and Technology, Sun Yat-sen University, Zhuhai 519082, China

[6] Guangdong Provincial Key Laboratory of Water Quality Improvement and Ecological Restoration for Watersheds, Institute of Environmental and Ecological Engineering, Guangdong University of Technology, Guangzhou, China

Correspondence: Wenpeng Lin; E-mail: linwenpeng@shnu.edu.cn

Abstract: *Spartina alterniflora*, an invasive plant, was introduced to the Chinese coastal zone in the early 90s. As an eco-engineering species, *S.alterniflora* not only alters saltmarsh species distributions, previously described as habitat degradation, but it also plays a vital role in coastal protection, especially for the development of recently emerged intertidal shoals. To provide a reference for coastal management under global change, we quantified the impact of the invasion process on provided ecological and coastal protection functions, exemplified at the emerging Jiuduansha Shoals (JDS) in the Yangtze Estuary. Results obtained by high-precision satellite monitoring and numerical modelling showed that the establishment and growth of *S.alterniflora* can exert considerable changes on local environment. The invasion of *S.alterniflora* to JDS wetland can be divided into three distinct phases, (1) establishment 1998~2003, (2) expansion 2003~2009, and (3) dominant 2009~2018 stages according to the changes in saltmarsh composition. Spatially, *S.alterniflora* continuously replaced *Scirpus mariqueter*, forcing *S.mariqueter* and *Phragmites australis* slowly to the lower and higher intertidal habitats, respectively. Notably, *S.alterniflora* expansion was the main driver that contributed to over 70% of recent JDS wetland expansion even under sediment deficit conditions. Established *S.alterniflora* marsh (directly) dampens more waves because of aboveground stems, but it also causes more accretion and indirectly leads to higher "morphological" wave dampening. Thus, it increases coastal defense provided by the saltmarsh in the context of sea-level rise and strengthening storms. In conclusion, the role of *S.alterniflora* invasion to the local environment under global changes is controversial. For sustainable coastal management, we need context-dependent *S.alterniflora* management to maximize the benefit of coastal protection and minimize the impact on local ecology, especially in sediment-starving estuaries with expected coastline retreat.

Keywords: *Spartina alterniflora* invasion; random forest (RF) classifier; numerical modelling; ecological impact; coastal protection; climate change.

1 Introduction

Coastal wetlands play a vital role in the global carbon cycle by reducing greenhouse gas emissions and sequestrating carbon in the sediment bed (Bauer et al., 2013; Schwarz et al., 2022). However, biological invasions to coastal wetlands are predicted to increase as a consequence of climate change (Parepa et al., 2013), and human interventions have been one of the most crucial environmental issues impacting local species communities and ecological functions (Meyerson and Mooney, 2007). *Spartina alterniflora*, globally is the most dominant herbaceous halophytic plant primary colonizer of coastal intertidal wetlands and the most common invasive saltmarsh in Chinese coastal areas (Liao et al., 2007; Liu et al., 2018; Strong and Ayres, 2013). The Jiuduansha Shoals (JDS) are the largest uninhabited island complex in the Yangtze Estuary, covered by extensive saltmarshes (Wei et al., 2016). The isolated wetland complex is the biggest nature reserve in the Shanghai area and serves as an essential link in the Australia-Asia-Siberia international waterfowl migration chain (Ma et al., 2014). It moreover provides other ecosystem services such as carbon sequestration, micro-climate regulation, and water purification for surrounding cities (Tang et al., 2011). However, since the majority of the above-described ecosystem services are linked to endemic saltmarsh vegetation, it is critical to monitor and evaluate the environmental impact caused by the *S.alterniflora* invasion.

Currently, the saltmarsh species of JDS wetland is dominated by *Phragmites australis*, *S.alterniflora*, and *Scirpus mariqueter*, co-existing with low-densities of *Zizania latifolia*, *Solidago canadensis,* and *Tripolium vulgare* (Lin et al., 2015). *S.alterniflora*, characterized by relative high salt tolerance (up to 34 ppt) and utilizing ammonium (NH_4^+) as its main nitrogen (N) source (Hessini et al., 2013; Hessini et al., 2017), was initially introduced to China in the 1960s as an eco-engineering plant to combat coastal erosion (Liu et al., 2018). The impact of the *S.alterniflora* introduction and invasion on the Chinese coastal environment has been widely recognized (Buckley and Han, 2014), ranging from reduced erosion and increased wetland extents to negative impacts on local flora and fauna communities (Huang and Zhang, 2007; Ma et al., 2015; Zhou et al., 2009). Specifically, *S.alterniflora* may exert stresses on the local saltmarsh species with its dense, fast-growing root network, which was linked to its ability of high N-assimilation rates regardless of salinity (Hessini et al., 2009; Hessini, 2022). The initial intention of introducing the ecological engineering plant *S.alterniflora* was to protect the coastline through its ability to trap sediments (Chung, 2006). In fact, *S.alterniflora* has proved to be very effective in promoting accretion and thereby played a positive role in trapping marine carbon (Liao et al., 2007) and protecting fragile coastlines from erosion by waves and tides (Kirwan et al., 2016; Temmerman et al., 2013). Recent studies all underline the negative impact of *S.alterniflora* on the sustainable development of local flora and fauna communities (Liu et al., 2018; Ma et al., 2014; Ma et al., 2015; Yang and Chen, 2021; Yuan et al., 2014), irrespective of its potential benefits for coastal protection of erosional coastlines. This becomes especially important considering the global estuaries are more and more stressed through, reduced riverine sediment supply (Syvitski et al., 2009), increasing rates of sea-level rise (Kirwan et al., 2016), and expected increases in storm frequency and magnitude (Erikson et al., 2018). A comprehensive evaluation of the effect of *S.alterniflora* invasions to the local wetland ecosystem, exemplified at the estuarine wetland of JDS in the context of global changes, is therefore urgently necessary (Buckley and Han, 2014).

JDS is an alluvial inter-, supra tidal island complex consisting of wetland and mudflat habitats, which are governed by highly-dynamic hydraulic forcing through tides, waves, and episodic storms (Wei et al., 2016; Zhang et al., 2021). Although many studies have investigated the impact of *S.alterniflora* invasions on local saltmarshes in the Yangtze Estuary, there still lacks a comprehensive integration of biotic and abiotic dimensions (Chung, 2006; Tang et al., 2011; Zhou et al., 2009). Previous studies on the JDS wetlands investigated the trajectory of the *S.alterniflora* invasion using multispectral remote sensing products (Huang and Zhang, 2007). Recently, a high-precision vegetation interpretation of JDS wetland was performed using auto-classification of the decision tree classifier considering plant multi-temporal phenological characteristics, and the accuracy was improved to 87.17% (Lin et al., 2015), nevertheless, the study period was relatively short (from 2010 to 2013). To explore the long-term influence of *S.alterniflora* invasion on the local environment comprehensively, an extended period of the *S.alterniflora* invasion trajectory needs to be studied, and its impact on the morphological development of the islands and additional coastal protection functions such as wave erosion and wave mitigation need to be assessed.

The development of high accuracy, rapid vegetation classification technology is crucial for the successful dynamic evaluation of *S.alterniflora* invasion using remote sensing. In recent years, object-oriented image analysis (OBIA), support vector machine (SVM), and random forest (RF) classifier have been widely used in the auto-classification of high spatial-resolution images (Breiman, 2001; Ouyang et al., 2011) and even hyperspectral images (Skowronek et al., 2017; Zhang and Xie, 2012) for saltmarsh mapping. On the other hand, machine learning techniques such as neural network classifier (NNC) and support vector data description (SVDD) have been applied to classify the intertidal saltmarsh and achieved higher accuracy when combined with auto-classifiers (Gong et al., 2021; Liu et al., 2018; Wang et al., 2007). It was shown that the RF classification method is superior to traditional classifiers (Breiman, 2001), and the accuracy is profoundly improved when combined with machine learning techniques (Lin et al., 2015; Zhang and Xie, 2012). Here, we use the NNC-supported RF classifier for long time-series Landsat TM data interpretation to map the dynamics of *S.alterniflora* expansion. Subsequently, we incorporate these vegetation patterns into a hydrodynamic model (TELEMAC2D), to assess the impact of the species invasion on currents, waves, and morphodynamics as demonstrated in (Zhang et al., 2018; Zhang et al., 2019; Zhang et al., 2021). The combination of state-of-art vegetation classification and hydrodynamic modelling enables us to accurately reproduce the storm wave propagation around JDS, thereby facilitating a novel integrated assessment of the *S.alterniflora* invasion on saltmarsh ecosystem services. More specifically, we can distinguish the indirect impact as increased sedimentation and direct effects as species-specific plant-flow interactions of the invasion on coastal protection and wave mitigation functions.

To this end, firstly, the remote sensing images in the recent 20 years were segmented, then the training samples were selected, and an RF classifier was performed to map the saltmarsh species. Secondly, the decadal variations of the JDS morphology and nearshore storm waves considering the effect of *S.alterniflora* accretion and wetland expansion were examined. Finally, we discuss the invasion pattern of *S.alterniflora* and the pros and cons of *S.alterniflora* impact on the local environment for a broader coastal management reference and in the context of climate change.

2 Materials and methods

2.1 Study area

Jiuduansha Shoals (JDS) wetland (between 31°03' to 31°17'N and 121°46' to 122°15'E), consist of four independent islands of Jiangyananansha, Shangsha, Zhongsha, Xiasha, and the nearby shallow shoals, is located in the Yangtze Estuary between the North and South Passage (Fig. 1). Chongming Island formed approximately 2,000 years ago, followed by Changxing Island approximately 500 years ago, both located on the northwest side of JDS. The four islands of JDS are estuarine alluvial islands that first emerged in the 1950s developed following the southeast movement of the maximum turbidity zone of Yangtze Estuary (Chen et al., 1979; Wei et al., 2016). So far, the area above the mean sea level has reached 421 km^2. As a relatively recently emerged mudflat island, its history is relatively short. However, the fast expansion of JDS tends to play an essential role in the mouth bar-barrier system of the Yangtze Estuary in the future. Currently, there are four main wetland species recorded in JDS wetland: *P.australis*, *S.alterniflora*, *S.mariqueter*, and *Z.latifolia* (Huang and Zhang, 2007; Lin et al., 2015). The JDS wetland has a northern subtropical monsoon climate, with an average annual temperature of 16 °C, summer temperatures average of 28 °C, and winters are cold, with an average temperature of 4 °C (Huang and Zhang, 2007). Average annual precipitation is approximately 1,200 mm, with 60% of rainfall occurring during May~September and several typhoons during summer and autumn (Huang and Zhang, 2007).

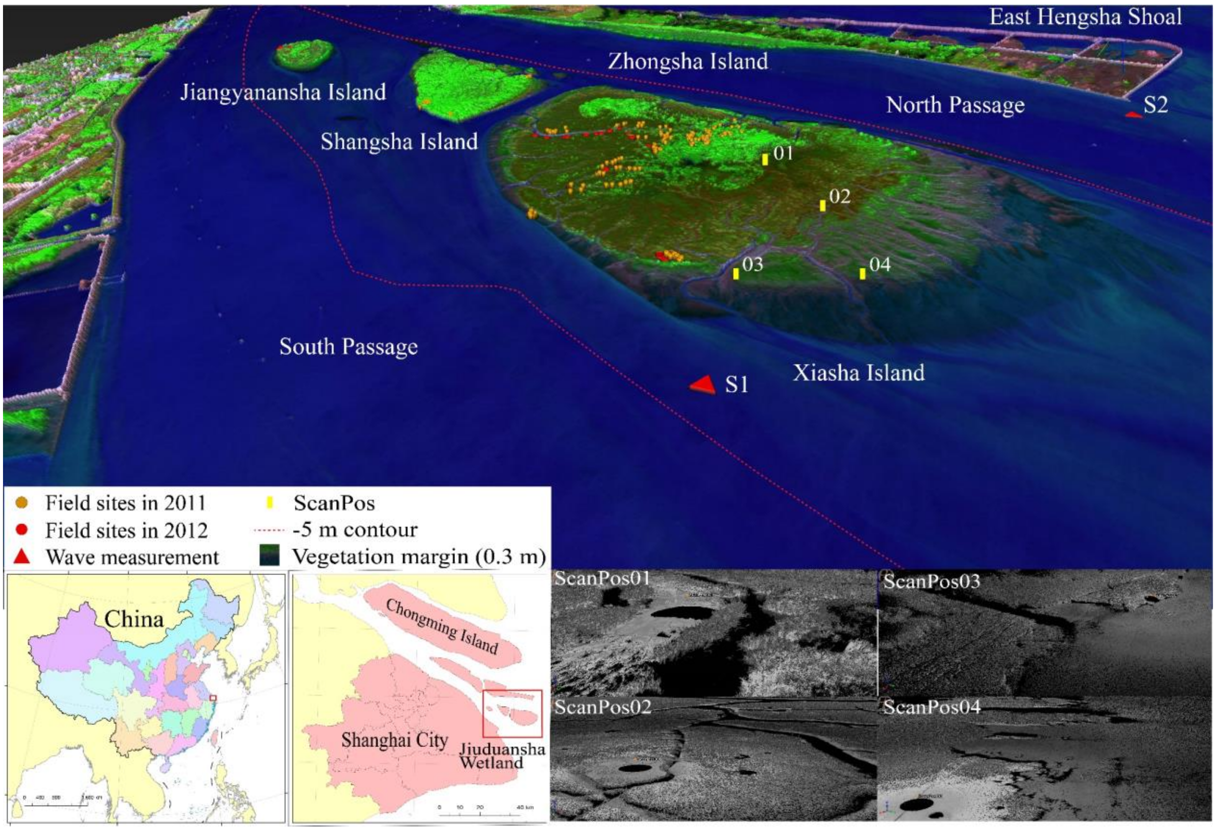

Fig. 1. Three-dimensional retrieval of the wetland morphology and saltmarsh in Jiuduansha Shoals (JDS) derived from stereo-pair aerial photogrammetry in 2019. The islands of Zhongsha and Xiasha were merged after 2000, with a tidal creek in between. The locations of field observation sites for vegetation survey, wave measurement, and RIEGL (VZ-200, the 3D Laser Measurement Systems) scanning were denoted with circles, triangles, and pillars, respectively.

2.2 Data acquisition and DEM building

2.2.1 Data acquisition

The Landsat TM/ETM/MSS satellite images are the most commonly used data sets for monitoring land cover changes (Gong et al., 2021), freely provided by the United States Geological Survey (USGS, https://glovis.usgs.gov/). Although other satellite products have higher resolutions (e.g., SPOT-5, IKONOS, Quickbird, and Worldview-2), Landsat

TM/ETM/MSS datasets possess the longest time-series, which is why they are routinely used for long-term land cover monitoring to avoid classification inconsistency caused by data heterogeneity (Liu et al., 2018). Since there were no Landsat5 and Landsat8 TM images in 2013, the striped Landsat7 TM images were used after de-striping (Gong et al., 2021). By considering the saltmarsh phenological characteristics, satellite images at different species phenological stages during the low-tide period with a minimum of clouds were selected, i.e., on the year of 1998, 2000, 2003, 2006, 2009, 2013, 2015, and 2018 (see Supplementary Table S1).

Frequently surveyed bathymetries with high accuracy are of major importance in identifying morphology evolution and performing hydrodynamic modelling in the shallow coastal area (Zhang et al., 2019). Here, a unique available seventeen navigation charts covering the study period by uninterrupted bathymetric surveys were collected, provided by Changjiang Estuary Waterway Administration Bureau (www.cjkhd.com). The surveys were taken annually, mainly in February and August, covering the area of JDS wetland and lateral passages (North Passage and South Passage) on a scale of 1:25,000 (before 2004) and 1:10,000 (after 2004). The vertical errors were declared to be 0.1 m using dual-frequency echo sounders for depth measurement and Trimble GPS devices for positioning (Wei et al., 2016). They were corrected from Theoretical Low-tide Datum (TTD) to National Height Datum (Huanghai 1985 datum) before mosaicing.

Other ancillary data includes monthly water discharge and suspended sediment flux measured at the Datong hydrological station, obtained from the Yangtze River Water Conservancy, the Bulletin of China River Sediment (www.cjw.gov.cn/zwzc/bmgb/). The Datong station, the closest hydrological station to Yangtze Estuary, is a reference station for many scholars studying the saltwater intrusion and sediment inflow in the Yangtze River (Chen et al., 2016; Zhang et al., 2019). The anthropogenic regulation of water and sediment from the upstream basin was proven to have an important influence on the downstream estuarine evolution (Mei et al., 2021), resulting in localized riverbed erosion and deposition, especially after the Three Gorges Dam (TGD) closure in 2003 (Cai *et al.* 2019). Therefore, it is essential to distinguish whether the change of water and sediment discharges or other factors dominate the recent JDS evolution in the Yangtze Estuary. In addition, the published historical JDS wetland area (Shen et al., 2006) in 1988 (12.9 km^2), 1990 (13.9 km^2), 1996 (19.9 km^2), and 1997 (24.4 km^2) was used as a reference to compare the JDS expanding rate before the introduction of *S.alterniflora* in 1997.

2.2.2 DEM building

Water depth images of subtidal areas derived from raw navigation charts were firstly scanned by DS-31200. Next, the water depth points were digitalized and geometrically corrected from Cartesian coordinates to WGS84 coordinates, then converted to Beijing54 coordinates in ArcGIS 10.1. Since the field-measured elevations in the wetland area were absent in the historical navigation charts, we supplemented the intertidal and supratidal topography based on the local saltmarsh surviving characteristics, i.e., the low-marsh, middle-marsh, and high-marsh are expected to most likely occupying the elevations ranging between 0.3~0.8 m, 0.9~1.3 m, and 1.4~1.8 m according to the vegetation survey conducted in the Yangtze Estuary (Cui et al., 2020). Data of supratidal, intertidal, and subtidal topography were then interpolated to a 50 m×50 m grid to build digital elevation models (DEMs) based on the ordinary Kriging spherical semivariogram model interpolation method. The historical variance of DEMs well reflected the wetland morphology and nearby channel evolutions in the years (month) 1998.9, 1999.2, 2000.2, 2001.2, 2001.8, 2002.2, 2002.8, 2003.8, 2004.8, 2005.2, 2006.8, 2007.2, 2008.11, 2009.5, 2011.8, 2013.11, and 2014.8 (see Supplementary Fig. S1). Subsequently, two depth contours of 0.3 m and -5 m, representing low marsh boundary and wind-wave penetration limit, were extracted and analyzed on area changes above the given depths as the envelopes of the corresponding contours.

2.3 Image segmentation, sample selection, and random forest (RF) classifier

TM remote sensing images were preprocessed by ENVI software for vegetation classification. Firstly, a standard pseudocolor image was produced by compositing the spectral bands of near-infrared (760-960 nm), red (620-690 nm), green (520-600 nm), followed by a geometric correction, radiometric calibration, and atmospheric correction (Lin et al., 2015; Liu et al., 2018). The image radiometric calibration and atmospheric correction, correcting the distorted electromagnetic radiation due to the atmospheric scattering and absorption, were executed by the FLAASH (Fast Line-of-sight Atmospheric Analysis of Spectral Hypercubes) model for accurate image retrieval. Next, image denoising and stripe removal were performed, if necessary, with ENVI plug-in tm_destripe unit (Lin et al., 2015). Finally, the images were preliminarily clipped to a narrower processing area.

The image segmentation method merged the adjacent pixels with similar colors into a unified object (Ouyang et al., 2011). Based on field surveys, the land coverage of the study area could be divided into six classes: *S.mariqueter*, *P.australis*, *S.alterniflora*, *Z.latifolia*, bare tidal flat, and water. To achieve that, firstly, the pure pixels in the same segmentation unit located on different islands were selected to create the six groups of representative training samples. Secondly, an image division and region-scale merging iteration were performed until the segmentation scale reached 30 and the merging scale was 10 when the result was the best. Finally, the RF (Random Forest) classifier was to perform classification via random selection from a forest composed of many non-parametric classifications and degrees of decision tree/CART (classification and regression tree). We can then refine the saltmarsh classification by establishing an extended normalized difference vegetation index (NDVI) database.

The detailed process of RF classification was as follows: firstly, an *n*-number of training samples were extracted from the original training samples using the bootstrap sampling technique and set the size of each sample consistent with the initial training sample. Secondly, an *m*-number of decision-tree models were established for the subsets of samples, which constituted the RF classifier; then, the decision trees were used to classify the test sample sets, and the prediction of each class was obtained. Finally, a vote on the results was to identify samples with the highest scores (Breiman, 2001). Generally, the ideal classification accuracy can be achieved using default parameters (Breiman, 2001; Lin et al., 2015). However, some studies showed the classification accuracy of the RF classifier was insensitive to parameter settings except for the number of decision trees (Zhang and Xie, 2012). In this study, the best classification accuracy with the maximum *Kappa* coefficient (Lin et al., 2015) obtained through experiments was when the depth of the decision tree was set to 100.

2.4 Hydrodynamic modelling

2.4.1 Model setup

The hydrodynamic modelling of wave propagation was simulated using TOMAWAC (Hervouet, 2007), a two-dimensional finite-element module of TELEMAC solving the balance equations of wave action density spectrum for deep and shallow water physics (Hervouet, 2007). The computational domain was delineated with unstructured irregular triangular mesh, covering the entire JDS, North Passage, South Passage, and a portion of the nearby coastal regions (Supplementary Fig. S1). A gradually increasing cell resolution from 200 m on the offshore to 20 m on the nearshore was constructed, resulting in finite element meshes of 25,600 nodes, approximately 50% located on and around JDS. Consistent with our previous studies on Nanhui Coast (Zhang et al., 2021) and Chongming East Shore (Chong et al., 2021; Mi et al., 2022) in the Yangtze Estuary, wave modelling was configured with implicit vegetation friction, depth-induced wave breaking, and white capping (Hervouet, 2007). The spectral frequency was discretized at 30 intervals, with a minimum frequency of 0.055 Hz, increasing equidistantly at 0.03 Hz (Zhang et al., 2021). A simplified Nikuradse roughness method combining vegetation and bottom friction was employed, which was proved effective after proper calibration by reproducing the physics of wave attenuation for implicit vegetation modelling (Mi et al., 2022; Willemsen et al., 2020).

Seventeen sets of triangular meshes, configured with historical bathymetries (Supplementary Fig. S1) and remote-sensing interpreted vegetation distribution of the same years, were prepared to model the wave characters. Water depth was corrected to the consistent datum of Huanghai 1985; for this reason, the datum needed to be uplifted by 3.5 mm/yr to account for sea-level rise (Chen et al., 2016; Church et al., 2004), which was shown to have considerable influences on the nearshore wave propagation (Zhang et al., 2021). The long-term effect of vegetation expansion on wave attenuation was examined by explicitly differentiating bottom frictions between saltmarsh and bare tidal flat. After substantial calibration (Chong et al., 2021; Mi et al., 2022; Zhang et al., 2019; Zhang et al., 2021) and validation with field measurements (referring to section 2.3.3), the adopted Nikuradse roughness length scale K_N for the typical saltmarshes *Z.latifolia*, *P.australis*, *S.alterniflora*, and *S.mariqueter* was set to be 0.15 m, 0.12 m, 0.08 m, and 0.014 m, respectively (Table 1). Shallow and deep shoals were set to be 0.002 m and 0.001 m, respectively, based on the bottom friction data of a comparable system (Wamsley et al., 2010). They were converted from Manning friction coefficients n typically representing marshes and subtidal shoals during typhoon conditions (Chong et al., 2021; Mi et al., 2022) using the conversion equation

$$K_N = H\, exp\left[-\left(1 + \frac{kH^{1/6}}{n\sqrt{g}}\right)\right], \qquad (1)$$

where g is gravity acceleration, *H* is water depth, and *K* is the von Karman constant (Wamsley et al., 2010). The scenario with vegetation was assumed to represent the summer condition with maximum aboveground biomass presented in JDS wetlands, demonstrating combined vegetation and tidal flat morphology induced wave attenuation. In contrast, the scenario without vegetation was assumed to represent the winter condition by removing the vegetation effect from the model using only the bare-mudflat bed friction, demonstrating only the morphological wave attenuation (Möller et al., 2014; Vuik et al., 2016).

Table 1. Vegetation metrics of dominant species in Jiuduansha Shoals (JDS) wetland and the applied bottom frictions for the hydrodynamic model.

Vegetation/landscape	Height/elevation (m)	Density (ind/m)	Equivalent rod diameter (m)	Canopy diameter (m)	Nikuradse roughness (m)
Z.latifolia	1.7~2.6	15~30	0.006~0.009	0.3~0.4	0.15
P.australis	1.8~2.5	76~132	0.005~0.008	0.2~0.3	0.12
S.alterniflora	1.5~1.6	280~344	0.007~0.008	0.03~0.04	0.08
S.mariqueter	0.31~0.72	50~1,160	0.001~0.002	0.01~0.03	0.014
Bare tidal flat	-1.5~0.3	–	–	–	0.002
Shallow shoals	-5~-1.5	–	–	–	0.002
Deep shoals	<-5	–	–	–	0.001

2.4.2 Scenario simulations

Three storm surge scenarios were designed to force the seaward boundary of JDS wave model (Table 2). The hydrodynamic boundary, consisting of tides and waves, was statistically derived from long-term numerical modelling in the Yangtze Estuary (Zhang et al., 2021). Firstly, the monthly maximum water level and significant wave heights (H_s) close to JDS, representing extreme events over 40 years (e.g., storm surge coincidence with the high astronomical tide), were extracted from the large-scale model (Zhang et al., 2021). Then, we applied suitable probability density functions (PDFs) by fitting the generalized extreme value (GEV), Gumbel, and Gamma distribution to the extracted waves, tides, and surges, respectively, according to the best choice of the Chi-Square test (Mi et al., 2022). Finally, the recurrence level of each hydrodynamic parameter was determined by using the exceedance probability of cumulative distribution function (CDF), whose reciprocal is defined as the return period T, representing an event occurring in any year with the probability of $1/T$ (Zhang et al., 2021). The purpose of using statistical return periods to drive the boundary conditions was to capture the magnitude of long-term trends indicative of possible future climate changes. The imposed parameters of surge heights, tidal levels, H_s, peak wave periods, and wave directions for the return levels 1/100 years, 1/200 years, and 1/500 years are shown in Table 2. All the parameters involved were given the 95% confidence interval range of the specified PDF distribution to perform uncertainty evaluations.

To allow a direct comparison between the seventeen sets of JDS wave models configured with varying historical vegetation and bathymetries, we forced them with the same hydrodynamic boundary conditions, which were interpolated onto the same triangular nodes of the TOMAWAC model at the seaward boundary. The warm-up period of hydrodynamic spin-up calculation was set to nine hours when the wave propagation around JDS became stable. Since the model parameter configurations and the hydrodynamic boundaries were kept the same for all runs, the difference in wave propagations at the nearshore was due to the changes in vegetation and bathymetry boundaries of JDS over time. The rise of water level due to storm surges on top of high tidal levels can increase above 3 m (Table 2), while the land elevation of JDS wetland was mainly below 2 m (Supplementary Fig. S1); hence all the saltmarshes on JDS were submerged and exposed to storm waves during typhoon conditions.

Table 2. Scenario designing parameters of hydrodynamic boundary condition (surge heights, tidal levels, significant wave heights (H_s), peak wave periods, and wave directions) for the

Jiuduansha wave model, with the applied mean value and 95% confidence interval.

Return level (P/year)	Surge (m)	Tide (m)	H_s (m)	Peak wave period (s)	Wave direction (°)
1/100	1.39 (1.11~1.73)	2.08 (2.07~2.09)	2.50 (2.20~2.96)	6.63 (6.16~7.19)	160
1/200	1.45 (1.16~1.81)	2.09 (2.08~2.10)	2.76 (2.35~3.30)	6.92 (6.37~7.61)	160
1/500	1.54 (1.23~1.91)	2.1 (2.09~2.11)	3.05 (2.53~3.76)	7.29 (6.62~8.15)	160

2.5 Performance evaluation

Machine-learning classifications of large-scale images may result in interpretation errors due to two main effects, (1) “different ground objects with the same spectrum” or (2) “the same ground object with different spectra”, hence calibration and validation are crucial to ensure its robustness. Since it was difficult to enter the core area of the JDS wetland in recent years, especially after establishing an international nature reserve, the classification results were validated using field observations obtained in 2011 and 2012. The precise locations of 97 and 56 sampling sites collected in 2011 and 2012 and the four RIEGL (VZ-200, the 3D Laser Measurement Systems) scanning positions are shown in Fig. 1. Classification results obtained around 2011 and 2012 were used to validate the applied algorithm directly. For other years, the ENVI5.3 classification accuracy assessment module performed validations by randomly generating 100 sample points for each land cover type evenly distributed in the study area. The actual land cover type of the corresponding ground locations was manually identified based on high spatial resolution images provided by Google Earth Pro Software. After that, the ENVI assessment module was used to evaluate the classification accuracy over 20 years.

Wave modelling data was validated based on hydrologic observations by two anchored boats, carried out synchronously from 8 to 10 June 2016. They were specifically designed to observe the nature of waves covering two tidal cycles (27 hours) during spring tide in the Yangtze Estuary. Two wave and tide sensors (SBE25) were used to measure the hydrologic parameters, including pressure, tide level, tide pressure, H_s, maximum wave height, mean period, peak period, and energy wave period. Critical parameters such as wave burst sampling rate and sampling period were set to 4 Hz and 10 min, respectively. The observed H_s were compared against the modelling results at the in-situ measurements S1, located at the north of east Hengsha Shoals, and S2, located at northeast JDS (Fig. 1). Both S1 and S2 were in the shallow water areas around JDS; hence the obtained results reflect the effects of bathymetry on shallow-water wave propagations.

The quantitative statistics criteria of root-mean-square error *(RMSE*), the mean-absolute error (*MAE*), and the *Skill* value were used to evaluate the wave modelling results (Zhang et al., 2021); P_{PA}, P_{UA}, P_{OA}, and *Kappa* coefficients were used to assess the RF classification accuracy (Lin et al., 2015). The *RMSE* indicates the magnitude of the error and is ideal to be zero. The MAE indicates normalized over-prediction or under-prediction of modelling to the observation and is ideal to be zero. A skill value of 1.0, 0.65~1, 0.5~0.65, 0.2~0.5, and <0.2 indicates perfect, excellent, very good, good, and poor model performance. P_{PA} is the classification precision; P_{UA} represents user precision; P_{OA} is the overall classification accuracy; *Kappa* coefficient refers to the similarity between sampling and RF classification.

3 Results

3.1 Accuracy of conducted analysis

3.1.1 Validation of plant species classification

Firstly, the three dominant species (i.e., *P.australis*, *S.alterniflora*, and *S.mariqueter*) interpreted from the 2013 TM image were compared with the field surveys carried out in 2011 and 2012. Results showed a high classification accuracy of 82.9% (see also P_{OA} in Supplementary Table S2). The misinterpreted points were all located in the vegetation transitioning zones with mixed vegetation species. Among these, the interpretation of *S.mariqueter* exhibited the lowest accuracy, mainly caused by the varying degrees of co-occurrence of *S.mariqueter* with other plant species. Overall, the total land cover classification accuracy of JDS wetland for the eight periods was up to 90%, and the *Kappa* coefficient was more than 0.89 (Supplementary Table S2). Among these, the classification accuracy of water and tidal flat was the highest, nearly 100%, which improved the overall classification accuracy. Although low-tide images were selected as much as possible, it is possible that some vegetation was still covered by seawater. In general, the overall classification accuracy was satisfying, suggesting that the RF classifier was appropriate for monitoring *S.alterniflora* expansion in the JDS wetland.

3.1.2 Validation of hydrodynamic model prediction

Wave modelling results were extracted and compared with field measurements at two distinct locations (Figs. 1, S2). Overall, the modelled H_s and phases compared well with the field measurement at sites S1 and S2. For the first peaks of S1 and S2, the wave modelling results were very reliable considering the small *RMSE* value (0.03 m), small *MAE* value (0.02 m), and high *Skill* score (0.99), while for the second wave peaks, we find an underestimation of H_s at S1 and a slight overestimation of H_s at S2 (see Supplementary Fig. S2). Overall, the *RMSE* value (0.09 m) and *MAE* value (0.08 m) were small, and the *Skill* value (0.8) remained high over the entire measurement period, suggesting a good fit between predictions and observations. In addition, the numerical modelling results were compared with the published H_s from European Centre for Medium-Range Weather Forecasts (ECMWF, www.ecmwf.int/) over the spring and neap tidal cycle. The numerical modelling was observed to capture the magnitude and cycle of wave variation following semi-diurnal tidal water-depth variations. In contrast, the inconsistency in the instantaneous wave height was due to the fine spatial-temporal resolution of TOMAWAC modelling (20 m × 15 s) compared with the relatively coarse spatial-temporal resolution of ECMWF data (25 km × 6 h), which were designed for global-scale study. Despite the inconsistency, the calculated *RMSE* (0.1 m), *MAE* (0.1 m), and *Skill* value (0.6) between TOMAWAC and ECMWF were reasonably accurate. In principle, the customized TOMAWAC wave modelling faithfully reproduced the key information of wave propagations over shallow waters around JDS.

3.2 Dynamics of *S.alterniflora* invasion from 1998 to 2018

Spatial-temporal mapping of the dominant saltmarsh species (i.e., *P.australis*, *S.alterniflora*, *S.mariqueter*, and *Z.latifolia*) from 1998 to 2018 (Fig. 2) provides an ideal time-series trajectory to observe dynamic vegetation evolution of the JDS wetland. The invasion of *S.alterniflora* on JDS is clearly visible, not only replacing the previous primary colonizer *S.mariqueter* but also accelerating the formation of high-marsh habitats with accompanied dominance of *P.australis* in the middle island where the land elevation is higher with less tidal inundation (Figs. 2, 3). Overall, *S.alterniflora* spread rapidly, with the total wetland area increasing from only 21 km^2 in 1998 to over 96 km^2 in 2018. During this period, we separate the *S.alterniflora* invasion into three distinct phases based on changes in proportion and ratios between invasive and native species (Fig.4): 1998-2003 representing the establishment stage when the proportion of *S.alterniflora* (6.6%) was smaller than any of other major native species (77.9% of *S.mariqueter* and 15.5% of *P.australis*); 2003-2009 representing the expansion stage when the proportion of *S.alterniflora* (37.4%) began to surpass one or two other major native species (34.1% of *S.mariqueter* and 28.4% of *P.australis*); 2009-2018 representing the dominant stage when the proportion of *S.alterniflora* (52.8%) exceeded the sum of other two native species (17.9% of *S.mariqueter* and 29.3% of *P.australis*). Different phases can moreover be clearly distinguished by looking at the ratios between invasive and native species, with low ratios during the establishment stage, ratios approaching one during the expansion stage, and ratios above one during the dominant stage.

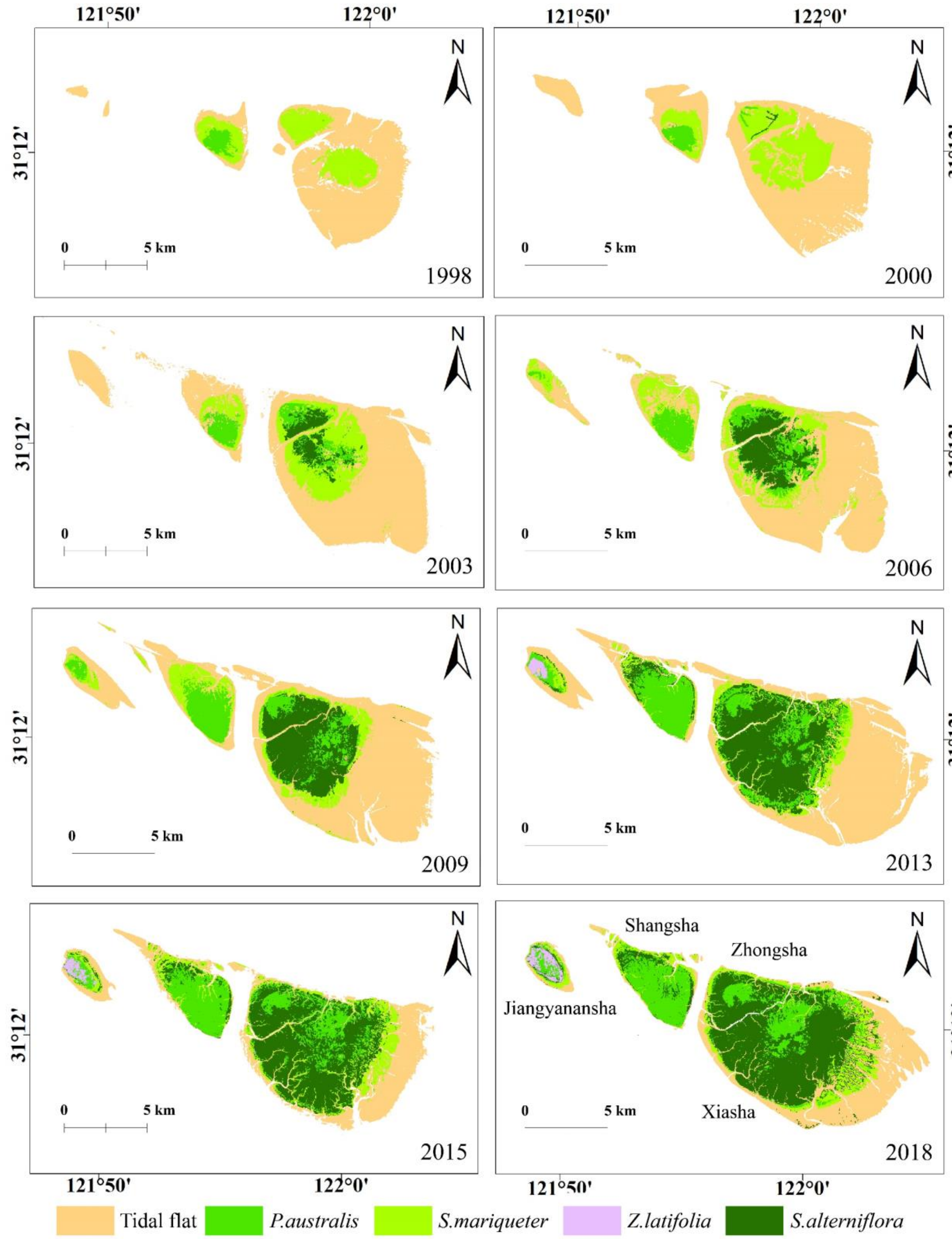

Fig. 2. The remote sensing retrieval of vegetation coverage in Jiuduansha Shoals (JDS) wetland and the spatio-temporal change of dominant plant species from 1998 to 2018.

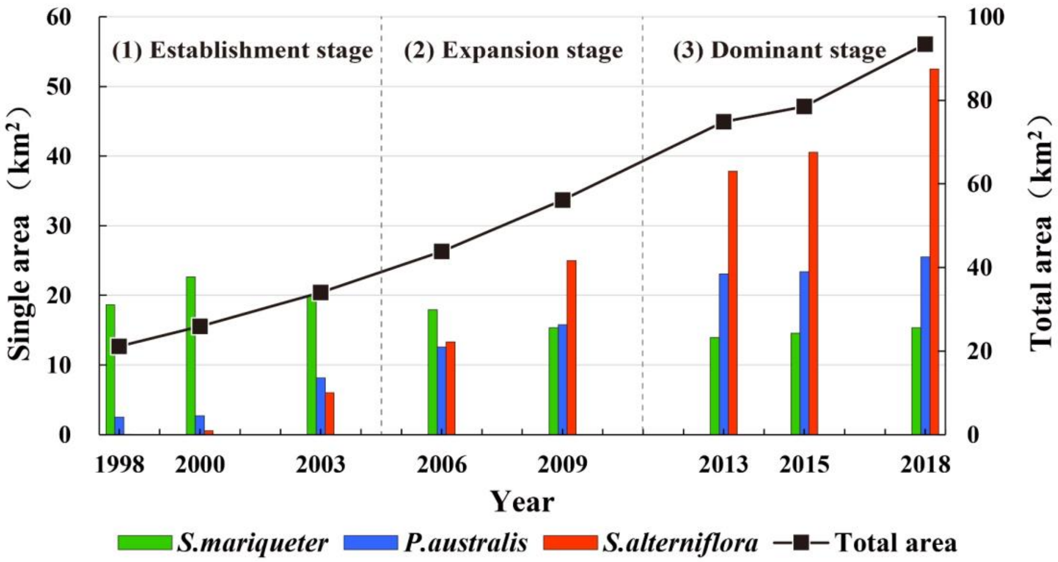

Fig. 3. Changes in vegetation area of main species in Jiuduansha Shoals (JDS) wetland over the past 20 years. Three phases of *S.alterniflora* invasion were divided according to the dominant plant composition, i.e., establishment stage 1998~2003, expansion stage 2003~2009, and dominant stage 2009~2018.

3.2.1 Temporal variation characteristics of *S.alterniflora* expansion

Establishment stage: In 1998, remote sensing interpretation detected no evident *S.alterniflora* distribution (Fig. 2). In 2000, a stripe of *S.alterniflora* emerged in the inner part of Zhongsha Island. *S.mariqueter* was still dominant, but colonization rates of *S.alterniflora* and *P.australis* started to increase. **Expansion stage:** A small patch of *S.alterniflora* in the inner part of JDS's main island became observable in 2003. The *S.mariqueter*, *P.australis*, and *S.alterniflora* accounted for 58%, 24%, and 18% of the total vegetation area (34 km^2), respectively. However, *S.alterniflora*'s expansion rate is 1.8-times higher than *P.australis,* increasing its coverage, but *S.mariqueter* remained dominant (Figs. 2, 3). **Dominant stage:** *S.alterniflora* became the largest population in the wetland starting from 2009. In the subsequent years (2009~2011), the artificial harvesting of *P.australis* promoted the root system spreading and slightly increased the expansion of *P.australis* by 30%. However, later in 2015, the growth of *P.australis* was leveled off due to the rapid expansion of *S.alterniflora*, which accelerated almost linearly starting from 2009 and continued throughout the dominant stage. While the area of *P.australis* and *S.mariqueter* remained unchanged during this period, partly due to human management. By 2018, the area of *S.alterniflora*, *P.australis*, and *S.mariqueter* was 52.5 km^2, 25.5 km^2, and 15.4 km^2, respectively, when *S.alterniflora* accounted for 54.9% of the total vegetation area, becoming the single dominant species of JDS wetland (see Fig. 2).

3.2.2 Spatial variation characteristics of *S.alterniflora* expansion

Establishment stage: *S.alterniflora* could not be identified on the remote sensing images in 1998 when only a few strip-shaped *S.alterniflora* were observed in Zhongsha Island after two years in 2000. During this phase, the JDS vegetation was mainly *S.mariqueter*, widely distributed in Shangsha, Zhongsha, and Xiasha islands. The second dominant species, *P.australis*, was widespread in southern Shangsha Island and a few in northern Zhongsha Island, mainly in a band-shaped pattern due to artificial cultivation, which was then expanded to the south and east directions meeting with *S.alterniflora* expanding from north and east directions in Zhongsha Island. Until 2003, the vegetation of Zhongsha-Xiasha Island was changed by the spreading of *P.australis* and *S.alterniflora*, both of which were distributed in a patch pattern, occupying the original niche of *S.mariqueter*. **Expansion stage:** Beginning in 2006, *S.alterniflora* spread on Zhongsha-Xiasha Island and competed with the local species, which largely pushed *P.australis* to the central higher parts of the islands and, at the same time, inhibited the growth of *S.mariqueter* at the island margins. It was also because of the spreading

S.alterniflora that removed the *S.mariqueter* around the creeks of Xiasha Island. As a result, *P.australis* mainly occupied the high tidal flat of JDS. The middle and low tidal flat was mixed with *S.alterniflora* and *S.mariqueter*. Meanwhile, a small patch of *P.australis* and *S.mariqueter* appeared on Jiangyanansha Island. Such spatial distribution pattern continued until 2009 when *S.alterniflora* became the dominant species and occupied the main ecological niche of JDS, where the overall distribution pattern was not changed. **Dominant stage:** the prevalence of *S.alterniflora* was accelerated in Zhongsha and Xiasha Island starting from 2013. On the fringes of Jiangyanansha Island and northern Shangsha Island, zonal distribution of *S.alterniflora* emerged potentially through seed propagules. Meanwhile, *P.australis* and *S.mariqueter* occupied the central and margin of Jiangyanansha Island, mixed with *Z.latifolia* on the high tidal flat. Since 2015, the coverage of *S.alterniflora* in Shangsha Island increased profoundly and spread to the tidal creeks among the *P.australis* in 2018. Meanwhile, the proportion of *S.mariqueter* present on the northern and eastern part of Shangsha Island and the tidal creeks of Zhongsha and Xiasha Island gradually reduced due to increasing dominance of *S.alterniflora* and the erosion.

3.3 Dynamics of JDS morphology and hydrology following *S.alterniflora* invasion

The changes in JDS morphology (Figs. 4, 5) and wave height (Figs. 6, S3) following the wetland expansion also presented stepwise changes, which we present with respect to the above indicated *S.alterniflora* invasion stages (Fig. 3). The start and end time of each phase and the related JDS morphology change are represented in respect to both sediment accretion volume within the three main wetland species and the envelope areas above 0.3 m and -5 m contours, reflecting the saltmarsh water boundary and the wave penetration limit. The modelled wave height followed the changes in morphology and vegetation colonization varying over space but overall showed the increasing wave attenuation in response to *S.alterniflora* expansion.

3.3.1 Morphology variation characteristics of JDS

Establishment stage: *S.mariqueter* was the main driver for wetland accretion (Fig. 5). Over this short period strong accretion and slight erosion were observed for shallow and deep parts of JDS (Fig. 4). The areas above 0.3 m contour (the sheltered shores) increased at a rate of 4.28 km^2/yr, but the areas above -5 m contour (the exposed shores) decreased at a slight rate of -0.37 km^2/yr (Fig. 4). Among the overall linear tendency, a relatively large scattering of the annual area change was observed, with a deviation of determination coefficient R^2=0.07 and R^2=0.003 for the area above 0.3 m and -5 m, respectively. The large fluctuation in morphology was potentially linked to the limited ecological engineering function of the saltmarsh, and thereby hydrodynamics dominated the morphological evolution. **Expansion stage:** The ecological engineering function of *S.alterniflora* gradually gained influence, although *S.mariqueter* was still the main driver of the wetland accretion because *S.mariqueter* dominated (Fig. 5). Areas above both 0.3 m and -5 m contours increased continuously, among which areas above the saltmarsh water boundary (0.3 m) grew at a rate of 4.18 km^2/yr, and the areas above the wave penetrating limit (-5 m) presented the most significant increase with a rate of 4.71 km^2/yr (Fig. 4). Starting with a small original wetland area (105 km^2 in 2003), JDS expanded by 23% by year 2009, with the higher the shoals, the faster the expansion, while erosion occurred sporadically and was usually not severe (Fig. 4), reflecting the effect of vegetation on tidal flat accretion and sediment consolidation. **Dominant stage:** *S.alterniflora* cover exceeded *S.mariqueter* and became the primary driver of JDS accretion (Fig. 5). Significant changes appeared in the seaward half of the JDS wetland due to saltmarsh accretion, and high-speed wetland expansion was dominant in this phase, making this stage the most dramatic accretion stage at a rate of 3.75 million m^3/year (Fig. 5). In contrast, the area above the -5 m contour turned from rapid expansion to large fluctuation with a negative slope of -0.43 km^2/yr (Fig. 4). Thus the expansion of JDS wetland was likely caused by sediment redistribution from the erosional lower part of the shallow shoals. Despite the overall increasing tendency in area, the magnitude varied in different depths, reflecting the deep and shallow shoals of JDS had discrepancies in responding to the wetland and *S.alterniflora* expansion.

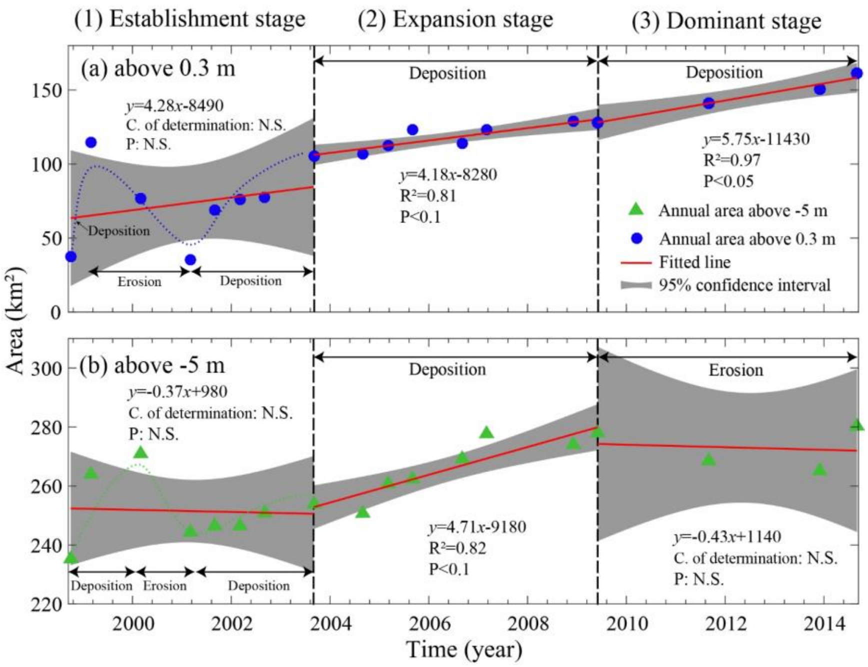

Fig. 4. Inner-stage area change of Jiuduansha Shoals (JDS) during the three phases of *S.alterniflora* invasion: (a) the area above the saltmarsh water boundary of 0.3 m contour, (b) the area above wave penetrating limit of -5 m contour. The trend line of linear fitting and 95% confidence interval during each phase were depicted with the solid red line and gray shadow surface.

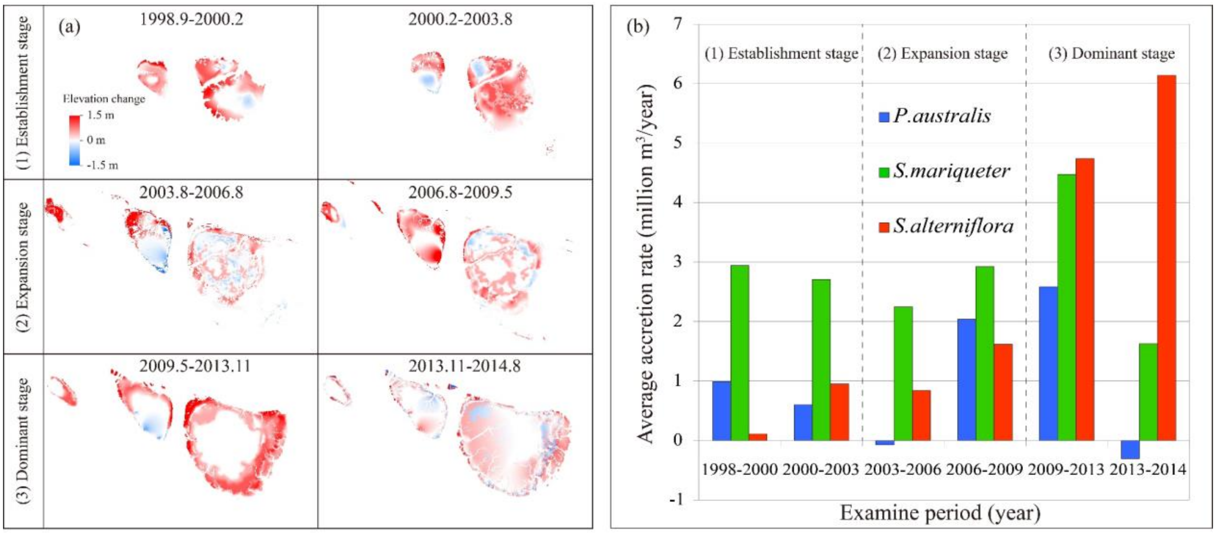

Fig. 5. Detailed morphology evolution of Jiuduansha Shoals (JDS) wetland for the area above 0.3 m: (a) sediment deposition and erosion depth in the vegetation coverage area during each examine period, (b) yearly average sediment volume accretion rate (negative is erosion) for the three main wetland species during each examine period.

3.3.2 Wave variation characteristics of JDS

Establishment stage: During the modelled 200-yr return period storm conditions, wave propagation caused significant wave height between 1 m to 2 m approaching the shallow area of JDS wetland (Fig. 6a, b). Chorochromatic mapping showed that high waves were convex to the islands, indicating high storm waves will directly approach the wetlands during storm surges. Even higher waves were observed at the exposed shores (above -5 m) than the nearby deep channels, probably due to the bathymetry-wave interaction occurring when vegetation was absent at the shallow shoals. The wave attenuation observed near the foreshore was due to depth-induced wave breaking, which was at least partly assisted by the existence of saltmarsh, stabilizing the bathymetry. **Expansion stage:** A medium storm wave height between 0.7 m to 1.2 m was observed at the sheltered shores (above 0.3 m) and 1.2 m to 2 m at the exposed shores

(Fig. 6c, d). Chorochromatic mapping showed high waves were flatted and distributed parallel to the JDS, indicating that the storm wave was attenuated at the frontier of wetland during storm conditions. The averaged wave height at the sheltered shores compared with the initial phase of 1998 during winter conditions (Supplementary Fig. S3b) reduced moderately between 25% to 30% if only considering the JDS indirect morphological wave attenuation (Supplementary Fig. S3g), and further reduced by 30% to 35% considering also vegetation-induced direct wave attenuation (Supplementary Fig. S3f). **Dominant stage:** The storm waves were much lower, ranging between 0.2 m to 0.6 m at the sheltered shores and 0.6 m to 2 m at the exposed shores, following the expansion of JDS Island (Fig. 6e, f). Chorochromatic mapping showed high waves were concave to the JDS, indicating that the expanded wetlands and shallow shoals effectively reduced the waves. The averaged wave height at the sheltered shores compared with the initial phase of 1998 during winter conditions (Supplementary Fig. S3b) reduced largely between 55% to 65% if only considering the JDS indirect morphological wave attenuation (Supplementary Fig. S3k), and further reduced by 20% to 30% considering the direct vegetation-induced wave attenuation (Supplementary Fig. S3j).

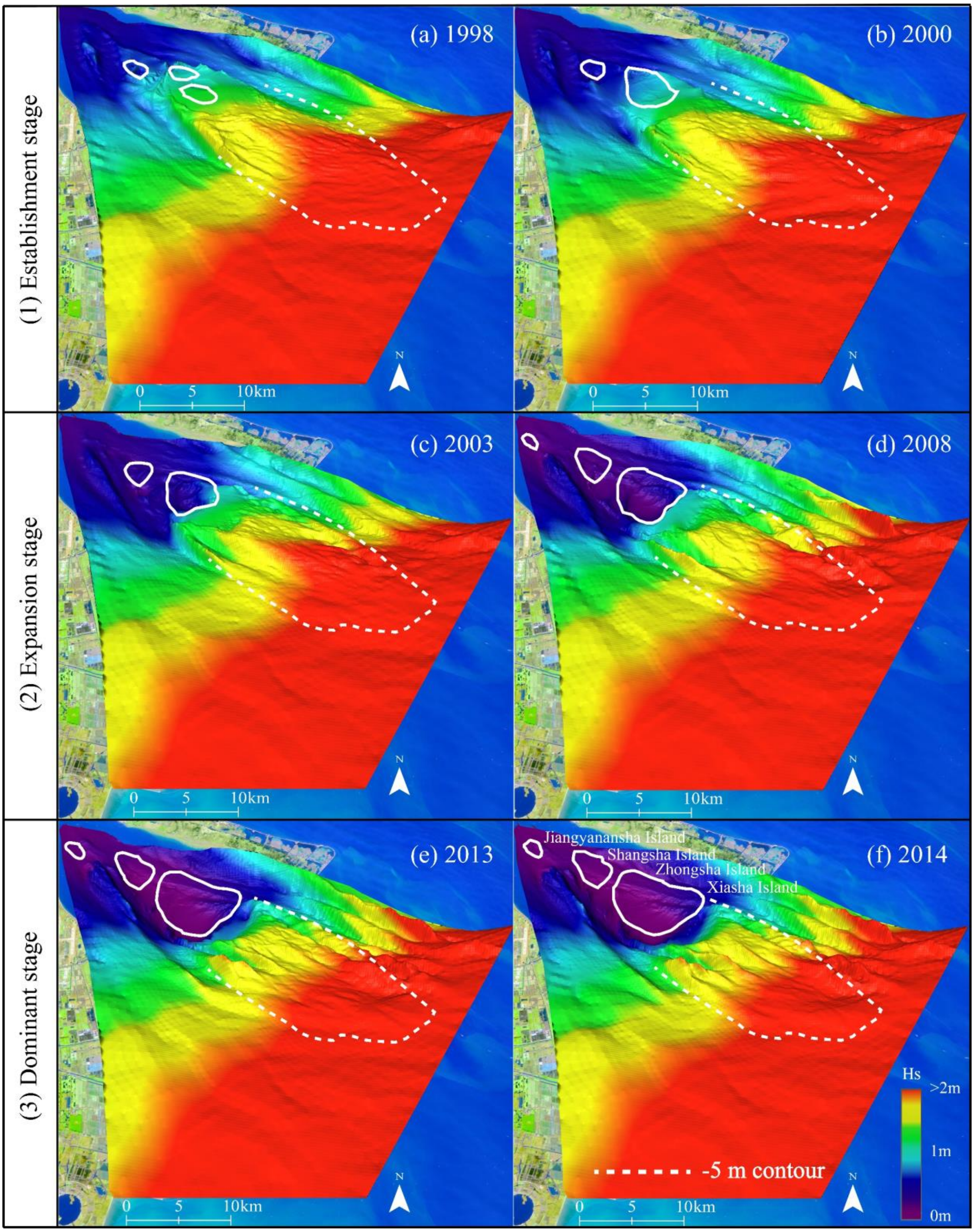

Fig. 6. The historical variation of significant wave heights (H_s) modelled using fixed hydrodynamic boundary conditions during storm surge conditions following the three phases of *S.alterniflora* invasion. H_s within -5 m contour, denoted by both colors and vertical elevations,

show a noticeable decrease trend following the expansion of Jiuduansha Shoals (JDS), especially in the wetland coverage area above 0.3 m contour.

3.4 Statistics of wetland expansion and wave mitigation following *S.alterniflora* invasion

Under the influences of river discharge and sediment deposition, the alluvial shoals of JDS constantly expanded over the past 20 years (Fig. 2). To disentangle whether hydrologic factors (e.g., riverine sediment supplies) or ecological factors (e.g., *S.alterniflora* invasion) dominate the recent expansion of JDS, the temporal change of the hydrological and ecological characteristics were compared. More specifically, we compared the sediment transport volume at Datong station with the change of JDS wetland area, invaded by *S.alterniflora* over the last 30 years (Fig. 7). Before the introduction of *S.alterniflora* from 1988 to 1998, the JDS wetland area increased relatively slow with an average rate of 1.2 km^2/yr, although the supplied sediment discharge volume was at its largest (~350 million ton/yr). However, in the recent 18 years, the provided sediment discharge volume decreased by two-thirds to only ~120 million ton/yr, but the JDS wetland area tripled its expansion rate to 3.0 km^2/yr and dramatically increased in total wetland area by 70 km^2 from 2000 to 2018, of which over 70% (52 km^2) was linked to the *S.alterniflora* area expansion (Fig. 7). *S.alterniflora*, the eco-engineering plant, consequently seems to play a dominant role in the recent expansion of JDS island, which showed almost no correlations with the change in annual river sediment supply (Fig. 7).

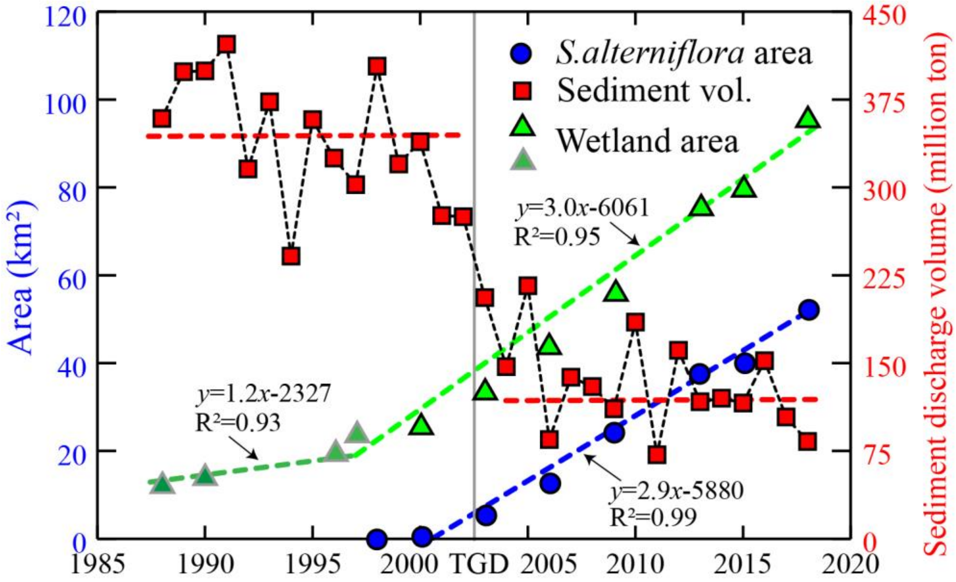

Fig. 7. Comparison of Jiuduansha Shoals (JDS) wetland area (green triangles) with the variation of critical driving factors, e.g., sediment supplies (red rectangles) and *S.alterniflora* invasion area (blue circles) in recent 30 years. The historical JDS wetland area before the introduction of *S.alterniflora* is shown in dark green triangles. TGD means the operation of Three Gorges Dam in 2003.

Wave mitigation by JDS wetland consists of vegetation-expansion-induced wave mitigation and morphology-accretion-induced wave mitigation. For comparison, the significant wave height, H_s, at the JDS wetland was examined from 1998 to 2014 using the area of the 2018 wetland boundary (see Supplementary Fig. S4). Predicting the wave attenuations of JDS during summer, assuming maximum aboveground biomass, demonstrates a combined vegetation and tidal flat induced wave damping. Notably, wave height reduction before 2006, when *S.mariqueter* was dominant, was between 0.7~1.1 m, while wave height reduction after 2009, when *S.alterniflora* was dominant, was down to 0.3~0.7 m (Supplementary Fig. S4a). In contrast, modelling wave attenuation during winter by removing the vegetation effect from the model, we quantified the role of indirect wave damping due to only the shallow water effect

(Supplementary Fig. S4a). The difference between winter and summer wave height reflected the wave mitigation only caused by vegetation, and the difference in winter wave height over time (e.g., relative to the starting year 1998.9 as the base case) reflected the effect of wave mitigation caused by tidal flat accretion (Supplementary Fig. S4a). Statistical analysis shows a comparable wave attenuation capacity between vegetation and shoal accretion effects (Supplementary Fig. S4b); both showed increasing over time following the stages of *S.alterniflora* expansion, with an increased rate of 0.0148 m/year and 0.0218 m/year, respectively.

4 Discussion

4.1 Invasion pattern of *S.alterniflora*

A zonal vegetation distribution of *P.australis–S.alterniflora–S.mariqueter* occupying the ecological niche of high–middle–low tidal flats respectively was observed in the JDS wetland (Fig. 2). Throughout the observed 20-year invasion, *S.alterniflora* continuously replaced *S.mariqueter*, meanwhile, *S.mariqueter* and *P.australis* were slowly driven towards lower and higher elevations, forming a distinct zonal vegetation pattern (Fig. 8). The restricted distribution of native species was due to being outcompeted by *S.alterniflora*. However, remaining habitats were also characterized by different environmental conditions in salinity and flooding frequency along the tidal flat elevation under cyclic tidal submerging (Gong et al., 2021). Specifically, the soil salinity increased with the rise of tidal flat elevation and then decreased when submerging was absent; hence the salinity was the highest where submerging was less frequent but evaporation was intensive (Khanna et al., 2012; Vasquez et al., 2006). Adaptable to such an environment, the leaves of *S.alterniflora* were full of developed salt glands and special stomatal; hence *S.alterniflora* was more tolerant to salt and submerging than other saltmarsh species (Liao et al., 2007; Yang and Chen, 2021). Moreover, during the establishment phase before 2003, *S.alterniflora* was partly planted (Huang and Zhang, 2007), which would slowly develop a suitable soil condition able to recruit plants and outcompete *S.mariqueter*, especially due to its advantage of the longer growing season, since *S.alterniflora*'s growing season is from April to November and *S.mariqueter*'s growing season is from May to October (Schwarz et al., 2011). These characteristics made *S.alterniflora* a successful invader able to outcompete its native counterpart at mid-low tidal elevations.

Meanwhile, *P.australis* had a competitive advantage in low-salinity and low-submerging environments (Schwarz et al., 2011). Hence, the *P.australis* on Zhongsha and Xiasha Island spread directly to the high tidal flat. While, *S.mariqueter* showed strong adaptability to low tidal flat with higher submerging frequency (Gong et al., 2021; Huang and Zhang, 2007), mainly distributed on the fringes. According to dynamic satellite monitoring, the area of *S.mariqueter* showed a slight decrease before 2009 while that of *P.australis* was relatively stable after 2013 (Fig. 3). Even artificial interventions of planting *S.alterniflora* on the seaside of JDS during the establishment stage (Huang and Zhang, 2007), revealed that it was unable to invade high elevation occupied by *P.australis*, although *S.alterniflora* squeezed at lower elevation. On Shangsha Island, for example, *S.alterniflora* firstly invaded *P.australis* along the tidal creeks close to the middle of the island, where the tidal flat elevation was below 0.8 m; at higher elevations, such a trajectory was not observed. In contrast, during the dominant stage, seeds of *S.alterniflora* established between *P.australis* and *S.mariqueter* and replaced *S.mariqueter* by drifting over a short distance to the Jiangyanansha Island. Thereby demonstrating a more substantial impact of the *S.alterniflora* invasion on *S.mariqueter* than on *P.australis*. Nevertheless, *S.alterniflora* was a significantly stronger competitor than *P.australis* and *S.mariqueter* at the mid-low elevations according to monitoring results of the past 20 years, potentially by low elevation and higher salinity (Vasquez et al., 2006).

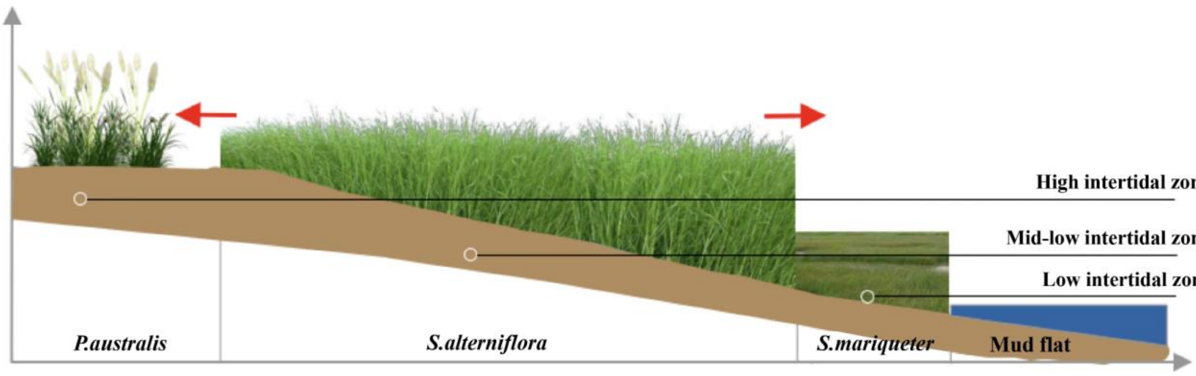

Fig. 8. The conceptual model summarizing the *S.alterniflora* invasion pattern to Jiuduansha Shoals (JDS) wetland.

4.2 Ecological engineering benefit of *S.alterniflora* invasion

4.2.1 Effect of *S.alterniflora* on the wetland expanding

The annual sediment transport volume at Datong station was measured to decrease dramatically, from 426 million tons in the 1970s~1980s to 337 million tons in the 1990s (Mei et al., 2021). Since the operation of TGD in 2003, the sediment input from the Yangtze River further reduced sharply, with peak values almost dropping by 70% (Wei et al., 2016). However, the area of the JDS wetland showed a continuous increase. Notably, there were periods when the area of JDS increased even more quickly after TGD operation, indicating little effect of TGD impounding on the recent JDS evolution. Earlier observations showed that JDS was in an initial subtidal phase from 1958 to 1971, then rapid accretion was experienced between 1971 and 1994 (Shen et al., 2006; Wei et al., 2016). However, after the 1990s, the absolute value of sediment transport to JDS decreased rapidly (Fig. 7). To cope with the possible future erosion under the low sediment expectation, *S.alterniflora*, as a green engineering plant, was introduced to Zhongsha Island in 1997 when it experienced 9711 typhoon and 1998 superfloods (Chung, 2006; Liu et al., 2018), so the initial accretion was not very effective (Fig. 5). Notably, after 2000, we observed an accelerated growth rate of the JDS wetland area, which was perfectly coincident with the rapid growth of the *S.alterniflora* area, with a coefficient of determination R^2=0.97 (Fig. 7). Therefore, it was reasonable to conclude that the introduction of *S.alterniflora* accelerated the recent expansion of the JDS wetland area.

Moreover, during the study period 1998~2014, a total volume of 55.8 million m^3 sediments was trapped by the wetland species (Fig. 5), in which 30% was trapped during the first eight years (1998~2006) when *S.mariqueter* was dominant, and 70% was trapped during the recent eight years (2006~2014) when *S.alterniflora* was dominant, proved the high efficiency of *S.alterniflora* on sediment trapping. *S.alterniflora*, as a green engineering plant, mainly affected the area change of sheltered foreshores (above 0.3 m) but played a slight role in the area change of exposed shores in the subtidal area (Fig. 4). Firstly, this was because saltmarsh is mainly located in the supratidal and upper intertidal zones, which attenuated tidal hydrodynamics and trapped sediments (Mi et al., 2022). Secondly, this also benefited from the proximal sediment sources of the mud center from the ocean (Wei et al., 2016), considering the sharp drop of river sediment supplies but slight changes in surrounding suspended sediment concentration (Mei et al., 2021). Concerning the deep waterway project (DWP) lies on the north of JDS, it was considered to influence JDS area changes in the lower shoals of the north edge and south edge

(Wei et al., 2016). Like riverine sediment flux, relative stable river discharge and weather conditions during 1998~2018 played a minor role in JDS growth (Zhang et al., 2018).

4.2.2 Effect of *S.alterniflora* invasion on the coastal protection

Coastal wetlands, consisting of intertidal flats and saltmarshes, can supplement conventional coastal defenses (Chong et al., 2021; Möller et al., 2014; Wamsley et al., 2010). The introduction of *S.alterniflora* to JDS was initially intended to protect the coastline by trapping sediments and mitigating wave heights (Chung, 2006; Liu et al., 2018). However, recent studies have been underling the negative impact of the *S.alterniflora* invasion on saltmarsh ecology, which should be set into context to direct (i.e., plant-wave interactions) and indirect (i.e., sedimentation) ramification of its ecosystem engineering strength (Yang and Chen, 2021; Yuan et al., 2014; Zhou et al., 2009). Based on long-term field observation and modelling, we showed the added value of coastal safety under all bio-geomorphological settings presented in JDS wetland, especially in recent years with the thriving of *S.alterniflora* (Figs. 3, 6). By comparing the summer and winter wave attenuations of JDS, we distinguished the respective wave damping due to shoal accretion and vegetation expansion (see Supplementary Fig. S4). Data showed that consistent with the three phases of *S.alterniflora* expansion, the wave mitigation by morphology showed three visible stages (Supplementary Fig. S4b): a large fluctuation of around 0.1 m during the establishment stage, a steady rise of around 0.2 m during the expansion stage, and a rapid rise of around 0.4 m during the dominant stage. Relating this to the sediment volume accreted by the three main wetland species (Fig. 5), we conclude *S.alterniflora* potentially attenuates more waves because of aboveground stems directly, but it also causes more accretion and, therefore, indirectly leads to higher “morphological” wave dampening, as discussed in previous researches (Loder et al., 2009; Mi et al., 2022).

Recently hybrid coastal defense measures are gaining popularity, consisting of a wetland in front of the dike, reducing wave energy and thereby providing a sustainable alternative to a conventional hard seawall. Following the thriving of *S.alterniflora*, the expanded wetlands and vegetation constitute effective coastal protection. Firstly, by dissipating hydrodynamic energy, suspended sediment was trapped in the saltmarsh, enabling fast expansion of the JDS wetland and the foreshore area (Vuik et al., 2016). Secondly, the expanded foreshore further dissipated wave energy due to the thick and dense *S.alterniflora* at the low water boundary (Garzon et al., 2019), consequently reducing the wave propagation to the inner Yangtze Estuary and relieving the pressure of seawall breaching behind the islands. Thirdly, saltmarshes were sustainable and in that they could cope, to some extent, with sea-level rise (Kirwan et al., 2016); thereby, it was a prerequisite for dealing with amplified storm flood risks due to climate changes (Zhang et al., 2021). In principle, saltmarshes and wetlands were self-adaptive for sustainable coastal management compared with conventional engineering measures (Möller et al., 2014; Vuik et al., 2016). The above-described function is still highly context-dependent. In the Yangtze Estuary, excess sediment supply led to a rapid expansion of wetlands on JDS once an elevation threshold was surpassed (Wei et al., 2016). Nevertheless, in sediment starved system, we would expect a much slower evolution and higher susceptibly to waves and erosion, e.g., in the Pearl River estuary in China and most US estuaries (Garzon et al., 2019; Mi et al., 2022), which makes it more difficult to predict the sustainability of coastal protection over climate change.

4.3 Potential implications for coastal management

The advantages and disadvantages of the *S.alterniflora* invasion to the local environment have brought broad debates under global changes (Buckley and Han, 2014; Chung, 2006; Gong et al., 2021; Liu et al., 2018). The direct negative effect of *S.alterniflora* on the JDS wetland was the gradual removal of *S.mariqueter*, e.g., in the southwest of Shangsha-Zhongsha Island and Xiasha creeks, causing threats to the stability of the local ecosystem to some extent (Vasquez et al., 2006). In addition, the invasion of *S.alterniflora* degraded the local habitats, reduced the food sources, and restricted the activities of some waterfowl, such as geese and ducks (Ma et al., 2011). In contrast, the invasion of *S.alterniflora* might benefit some other bird communities, such as *Locust ella pryeri* (Ma et al., 2014). Moreover, in the long run, *S.alterniflora* might have a negligible effect on the local bird and benthic communities due to long-term coevolution (Buckley and Han, 2014). For example, the number of *Porthesia similis* and *Laelia coenosa* had increased in the habitats of *S.alterniflora* in the nearby island of Chongming Dongtan wetland during the periods 2010~2015 (Ma et al., 2011).

Besides, a wide foreshore stabilized by *S.alterniflora* significantly contributes to coastal safety even under storm conditions. The densely populated *S.alterniflora* played an essential role in mitigating waves and promoting sedimentation, hence protecting coastlines (Garzon et al., 2019). By encouraging *S.alterniflora* spread in front of an already existing hard infrastructure (e.g., seawalls and dikes), the coastal protection function can be increased acting as a nature-based solution, which is gaining attention globally (Mi et al., 2022; Temmerman et al., 2013). By combining *S.alterniflora* and hard seawall, the needed width of *S.alterniflora*-accreted foreshore can be estimated in the hybrid defense design for defending against specific return levels of storms (Zhang et al., 2021); consequently, the height of the seawall could be lowered accordingly, which is considered the benefit of implementing nature-based solutions. As for managing the ecosystem impact, some researchers demonstrated increased bird biodiversity with the help of seasonally mowing the *S.alterniflora* (Ma et al., 2014). Hence multiple factors in the local environment should be considered comprehensively, rather than simply removing *S.alterniflora* rapidly. We thus propose a context-dependent evaluation of the *S.alterniflora* invasion incorporating ecological effects on benthic communities, bird species, and bio-morphodynamic effects benefitting coastal protection.

However, current insights on the coastal protection function of *S.alterniflora* marshes on the JDS wetlands are limited to scarce field studies due to its restricted accessibility. Here, the accuracy of the wave mitigation model was based on published ECMWF data and a limited number of field observations on significant wave heights measured close to the JDS wetland (i.e., on the two locations of S1 and S2, see Fig. 1). Moreover, an indirect wetland topography retrieval approach based on saltmarsh survival characteristics (Cui et al., 2020) may introduce limitations, for example, some saltmarsh species may be erroneously located in areas outside of the statistical elevation level (Cui et al., 2020). Last but not least, the main limitation of the conducted evaluation method is the assumption that aboveground plant biomass was rigid, thus neglecting the impact of stem flexibility on wave mitigation in our model simulations (Mi et al., 2022). However, no data on stem rigidity was available to incorporate effects without adding major uncertainties, such as spatial and temporal variations in saltmarsh characteristics, wave attenuation by flexible vegetation, and stability of vegetation under extreme wave forcing (Vuik et al., 2018). Despite those limitations, the adopted method gives a first-order estimation of the possibilities of nature-based risk mitigation in front of a wide foreshore stabilized by

S.alterniflora in the context of climate change.

The development of the *S.alterniflora* invasion in China reflects previous invasions at different wetlands areas around the world, such as the UK, the Netherlands (Oenema and DeLaune, 1988), France (Baumel et al., 2001), in New Zealand (Hubbard and Partridge, 1981), and in the US (Hacker and Dethier, 2006). A specific example is the introduction of *S.alterniflora* to the UK through shipping ballast in the nineteenth century, with led to its hybridization with native *Spartina maritima*, forming the cordgrass *Spartina anglica* (Ainouche et al., 2004) to become the dominant primary colonizer in European coastal wetlands. Here, the introduction in China leads to erosion mitigation and endemic species replacement. *S.alterniflora*, as an eco-engineering species, was initially introduced to the Bohai Gulf of China from the United States in the 1960s but now has spread over a range of 19° latitude along the eastern coast of China with its strong adaptability and spreading ability (Chung, 2006; Liu et al., 2018). Researcher and stakeholders alike are concerned that *S.alterniflora* fully occupy the niche present in the intertidal zone (Ma et al., 2011; Skowronek et al., 2017), influencing the ecological environment (Zhou et al., 2009) and threatening the biodiversity of the intertidal area (Ma et al., 2015). Owing that, *S.alterniflora* was recognized as a harmful invasion species and was removed on a large scale in southern China, but in northern China, it is still considered neutral to the environment for its siltation-promoting and carbon-sequestrating benefit (Chung, 2006; Gong et al., 2021). Especially because of climate change and the focus on removing carbon from the atmosphere, wetlands and fast-growing primary colonizers such as *S.alternflora* are considered major contributors to carbon sequestration (Bauer et al., 2013). Especially important for sediment-starving estuaries and deltas, such as Mississippi Delta, Pearl

River Delta, Mekong Delta, and Rhine Delta, with expected coastline retreats (Syvitski et al., 2009), a stabilizing species could mitigate future threats. We demonstrated an excellent siltation-promoting ability of *S.alterniflora* for the emerging island of JDS, thereby may provide rich food sources and habitats for fish, birds, and other animals in the newly developed wetland. We thereby demonstrate that labeling an invasion as advantageous or detrimental to the environment in the context of climate change is a multi-faceted endeavor.

5 Conclusions

S.alterniflora's man-made introduction and diffusion on the JDS is a good example of a potential invasion triggered by global environmental change. Based on high-precision saltmarsh classification and hydrodynamic modelling, a comprehensive evaluation of the invasion process, ecological impact, and coastal protection function of *S.alterniflora* in JDS were explored. Meaningful conclusions for coastal management under global changes were derived. According to nearly 20 years of satellite monitoring, it was found that the introduced species of *S.alterniflora* spread rapidly on JDS, occupied the ecological niche of native plants, and became the single dominant species during the recent decade, leading to changes in saltmarsh composition and benthic community.

In contrast, the examined response of JDS to storm waves delivered a continuous decline trend over space and time with the thriving of *S.alterniflora*. The expansion of *S.alterniflora* effectively prevented coastal erosion by tides and currents, hence extending the foreshore width and indirectly leading to higher morphological wave dampening. Specifically, the spreading of *S.alterniflora* contributed over 70% of the recent JDS wetland area increase, effectively resisting the disturbance of sharp riverine sediment decrease. Besides, the densely distributed *S.alterniflora* stems present at the foreshore effectively attenuated the storm wave height, thereby relieving the pressure of seawalls on coastal safety even with strengthening storm expectations. The self-adaptive saltmarshes on coastal protection by building up the tidal flat, valid for estuaries and coasts worldwide, can contribute to designing hybrid structures for coastal defense under future sea-level rises. Therefore, for sustainable coastal management under global changes, multi-factors in the local area should be considered, and we should develop scientific and effective management measures of *S.alterniflora* invasion to gradually restore the local environment meanwhile maintaining the advantage of nature-based coastal protection.

Acknowledgments

This research is supported by the National Natural Science Foundation of China (42171282 and 41701001), Shanghai Pujiang Program (21PJC096), China Postdoctoral Science Foundation (2018M630414), Open Research Fund of State Key Laboratory of Estuarine and Coastal Research (SKLEC-KF202201), and Natural Science Foundation of Shanghai (20ZR1441500). The data that support the findings of this study are available from the corresponding author upon reasonable request.

References

Ainouche, M.L., Baumel, A., Salmon, A., Yannic, G., 2004. Hybridization, polyploidy and speciation in spartina (poaceae). New Phytol 161 (1), 165-172. https://coi.org/https://doi.org/10.1046/j.1469-8137.2003.00926.x.

Bauer, J.E., Cai, W., Raymond, P.A., Bianchi, T.S., Hopkinson, C.S., Regnier, P.A.G., 2013. The changing carbon cycle of the coastal ocean. Nature 504 (7478), 61-70. https://coi.org/10.1038/nature12857.

Baumel, A., Ainouche, M.L., Levasseur, J.E., 2001. Molecular investigations in populations of spartina anglica c.e. Hubbard (poaceae) invading coastal brittany (france). Mol Ecol 10 (7), 1689-1701. https://coi.org/https://doi.org/10.1046/j.1365-294X.2001.01299.x.

Breiman, L., 2001. Random forests. Mach Learn 45 (1), 5-32. https://coi.org/10.1023/A:1010933404324.

Buckley, Y.M., Han, Y., 2014. Managing the side effects of invasion control. Science 344 (6187), 975-976. https://coi.org/10.1126/science.1254662.

Chen, J., Yun, C., Xu, H., Dong, Y., 1979. The developmental model of the changjiang river estuary during last 2000 years (in chinese with english abstract). Acta. Oceanol. Sin. 01 (01), 103-111.

Chen, W., Chen, K., Kuang, C., Zhu, D.Z., He, L., Mao, X., Liang, H., Song, H., 2016. Influence of sea level rise on saline water intrusion in the yangtze river estuary, china. Appl Ocean Res 54, 12-25. https://coi.org/https://doi.org/10.1016/j.apor.2015.11.002.

Chong, Z., Zhang, M., Wen, J., Wang, L., Mi, J., Bricker, J., Nmor, S., Dai, Z., 2021. Coastal protection using building with nature concept: a case study from chongming dongtan shoal, china. Acta Oceanol Sin 40 (10), 152-166.

Chung, C., 2006. Forty years of ecological engineering with spartina plantations in china. Ecol Eng 27 (1), 49-57. https://coi.org/https://doi.org/10.1016/j.ecoleng.2005.09.012.

Church, J.A., White, N.J., Coleman, R., Lambeck, K., Mitrovica, J.X., 2004. Estimates of the regional distribution of sea level rise over the 1950-2000 period. J Climate 17 (13), 2609-2625. https://coi.org/10.1175/1520-0442(2004)017<2609:EOTRDO>2.0.CO;2.

Cui, L., Yuan, L., Ge, Z., Cao, H., Zhang, L., 2020. The impacts of biotic and abiotic interaction on the spatial pattern of salt marshes in the yangtze estuary, china. Estuarine, Coastal and Shelf Science 238, 106717.

https://coi.org/https://doi.org/10.1016/j.ecss.2020.106717.

Erikson, L.H., Espejo, A., Barnard, P.L., Serafin, K.A., Hegermiller, C.A., O'Neill, A., Ruggiero, P., Limber, P.W., Mendez, F.J., 2018. Identification of storm events and contiguous coastal sections for deterministic modeling of extreme coastal flood events in response to climate change. Coast Eng 140, 316-330. https://coi.org/https://doi.org/10.1016/j.coastaleng.2018.08.003.

Garzon, J.L., Maza, M., Ferreira, C.M., Lara, J.L., Losada, I.J., 2019. Wave attenuation by spartina saltmarshes in the chesapeake bay under storm surge conditions. Journal of Geophysical Research: Oceans 124 (7), 5220-5243. https://coi.org/https://doi.org/10.1029/2018JC014865.

Gong, Z., Zhang, C., Zhang, L., Bai, J., Zhou, D., 2021. Assessing spatiotemporal characteristics of native and invasive species with multi-temporal remote sensing images in the yellow river delta, china. Land Degrad Dev 32 (3), 1338-1352. https://coi.org/https://doi.org/10.1002/ldr.3799.

Hacker, S., Dethier, M., 2006. Community modification by a grass invader has differing impacts for marine habitats. Oikos 113 (2), 279-286. https://coi.org/https://doi.org/10.1111/j.2006.0030-1299.14436.x.

Hervouet, J.M., 2007. Hydrodynamics of free surface flows: modelling with the finite element method. John Wiley & Sons, INC, New York.

Hessini, K., 2022. Nitrogen form differently modulates growth, metabolite profile, and antioxidant and nitrogen metabolism activities in roots of spartina alterniflora in response to increasing salinity. Plant Physiol Bioch 174, 35-42. https://coi.org/https://doi.org/10.1016/j.plaphy.2022.01.031.

Hessini, K., Hamed, K.B., Gandour, M., Mejri, M., Abdelly, C., Cruz, C., 2013. Ammonium nutrition in the halophyte spartina alterniflora under salt stress: evidence for a priming effect of ammonium? Plant Soil 370 (1), 163-173. https://coi.org/10.1007/s11104-013-1616-1.

Hessini, K., Kronzucker, H.J., Abdelly, C., Cruz, C., 2017. Drought stress obliterates the preference for ammonium as an n source in the c4 plant spartina alterniflora. J Plant Physiol 213, 98-107. https://coi.org/https://doi.org/10.1016/j.jplph.2017.03.003.

Hessini, K., Martínez, J.P., Gandour, M., Albouchi, A., Soltani, A., Abdelly, C., 2009. Effect of water stress on growth, osmotic adjustment, cell wall elasticity and water-use efficiency in spartina alterniflora. Environ Exp Bot 67 (2), 312-319. https://coi.org/https://doi.org/10.1016/j.envexpbot.2009.06.010.

Huang, H., Zhang, L., 2007. A study of the population dynamics of spartina alterniflora at jiuduansha shoals, shanghai, china. Ecol Eng 29 (2), 164-172. https://coi.org/https://doi.org/10.1016/j.ecoleng.2006.06.005.

Hubbard, J.C.E., Partridge, T.R., 1981. Tidal immersion and the growth of spartina anglica marshes in the waihopai river estuary, new zealand. New Zeal J Bot (19), 115-121.

Khanna, S., Santos, M.J., Hestir, E.L., Ustin, S.L., 2012. Plant community dynamics relative to the changing distribution of a highly invasive species, eichhornia crassipes: a remote sensing perspective. Biol Invasions 14 (3), 717-733. https://coi.org/10.1007/s10530-011-0112-x.

Kirwan, M.L., Temmerman, S., Skeehan, E.E., Guntenspergen, G.R., Fagherazzi, S., 2016. Overestimation of marsh vulnerability to sea level rise. Nat Clim Change 6, 253.

Liao, C., Luo, Y., Jiang, L., Zhou, X., Wu, X., Fang, C., Chen, J., Li, B., 2007. Invasion of spartina alterniflora enhanced ecosystem carbon and nitrogen stocks in the yangtze estuary, china. Ecosystems 10 (8), 1351-1361. https://coi.org/10.1007/s10021-007-9103-2.

Lin, W., Chen, G., Guo, P., Zhu, W., Zhang, D., 2015. Remote-sensed monitoring of dominant plant species distribution and dynamics at jiuduansha wetland in shanghai, china. Remote Sens-Basel 7 (8). https://coi.org/10.3390/rs70810227.

Liu, M., Mao, D., Wang, Z., Li, L., Man, W., Jia, M., Ren, C., Zhang, Y., 2018. Rapid invasion of spartina alterniflora in the coastal zone of mainland china: new observations from landsat oli images. Remote Sens-

Basel 10 (12). https://coi.org/10.3390/rs10121933.

Loder, N.M., Irish, J.L., Cialone, M.A., Wamsley, T.V., 2009. Sensitivity of hurricane surge to morphological parameters of coastal wetlands. Estuarine, Coastal and Shelf Science 84 (4), 625-636. https://coi.org/https://doi.org/10.1016/j.ecss.2009.07.036.

Ma, D., Ju, R.T., Li, B., 2015. Preference of laelia coenosa for native and introduced populations of invasive spartina alterniflora. Biodiversity Science 1 (23), 101-108.

Ma, Z., Gan, X., Cai, Y., Chen, J., Li, B., 2011. Effects of exotic spartina alterniflora on the habitat patch associations of breeding saltmarsh birds at chongming dongtan in the yangtze river estuary, china. Biol Invasions 13 (7), 1673-1686. https://coi.org/10.1007/s10530-010-9924-3.

Ma, Z., Gan, X., Choi, C.Y., Li, B., 2014. Effects of invasive cordgrass on presence of marsh grassbird in an area where it is not native. Conservation biology : the journal of the Society for Conservation Biology 28 (1), 150-158.

Mei, X., Dai, Z., Darby, S.E., Zhang, M., Cai, H., Wang, J., Wei, W., 2021. Landward shifts of the maximum accretion zone in the tidal reach of the changjiang estuary following construction of the three gorges dam. J Hydrol 592, 125789. https://coi.org/https://doi.org/10.1016/j.jhydrol.2020.125789.

Meyerson, L.A., Mooney, H.A., 2007. Invasive alien species in an era of globalization. Front Ecol Environ 5 (4), 199-208. https://coi.org/https://doi.org/10.1890/1540-9295(2007)5[199:IASIAE]2.0.CO;2.

Mi, J., Zhang, M., Zhu, Z., Vuik, V., Wen, J., Gao, H., Bouma, T.J., 2022. Morphological wave attenuation of the nature-based flood defense: a case study from chongming dongtan shoal, china. Sci Total Environ 831, 154813. https://coi.org/https://doi.org/10.1016/j.scitotenv.2022.154813.

Möller, I., Kudella, M., Rupprecht, F., Spencer, T., Paul, M., van Wesenbeeck, B.K., Wolters, G., Jensen, K., Bouma, T.J., Miranda-Lange, M., Schimmels, S., 2014. Wave attenuation over coastal salt marshes under storm surge conditions. Nat Geosci 7 (10), 727-731. https://coi.org/10.1038/ngeo2251.

Oenema, O., Delaune, R.D., 1988. Accretion rates in salt marshes in the eastern scheldt, south-west netherlands. Estuarine, Coastal and Shelf Science 26 (4), 379-394. https://coi.org/https://doi.org/10.1016/0272-7714(88)90019-4.

Ouyang, Z., Zhang, M., Xie, X., Shen, Q., Guo, H., Zhao, B., 2011. A comparison of pixel-based and object-oriented approaches to vhr imagery for mapping saltmarsh plants. Ecol Inform 6 (2), 136-146. https://coi.org/https://doi.org/10.1016/j.ecoinf.2011.01.002.

Parepa, M., Fischer, M., Bossdorf, O., 2013. Environmental variability promotes plant invasion. Nat Commun 4 (1), 1604. https://coi.org/10.1038/ncomms2632.

Schwarz, C., Ysebaert, T., Zhu, Z., Zhang, L., Bouma, T.J., Herman, P.M.J., 2011. Abiotic factors governing the establishment and expansion of two salt marsh plants in the yangtze estuary, china. Wetlands 31 (6), 1011-1021. https://coi.org/10.1007/s13157-011-0212-5.

Shen, F., Zhou, Y.X., Zhang, J., 2006. Remote-sensing analysis on spatial-temporal variation in vegetation on jiuduansha wetland. Oceanologia Et Limnologia Sinica 06, 498-504.

Skowronek, S., Ewald, M., Isermann, M., Van De Kerchove, R., Lenoir, J., Aerts, R., Warrie, J., Hattab, T., Honnay, O., Schmidtlein, S., Rocchini, D., Somers, B., Feilhauer, H., 2017. Mapping an invasive bryophyte species using hyperspectral remote sensing data. Biol Invasions 19 (1), 239-254. https://coi.org/10.1007/s10530-016-1276-1.

Strong, D.R., Ayres, D.R., 2013. Ecological and evolutionary misadventures of spartina. Annual Review of Ecology, Evolution, and Systematics 44 (1), 389-410. https://coi.org/10.1146/annurev-ecolsys-110512-135803.

Syvitski, J.P.M., Kettner, A.J., Overeem, I., Hutton, E.W.H., Hannon, M.T., Brakenridge, G.R., Day, J., Vörösmarty, C., Saito, Y., Giosan, L., Nicholls, R.J., 2009. Sinking deltas due to human activities. Nat Geosci 2, 681-686.

Tang, Y., Wang, L., Jia, J., Fu, X., Le, Y., Chen, X., Sun, Y., 2011. Response of soil microbial community in jiuduansha wetland to different successional stages and its implications for soil microbial respiration and carbon turnover. Soil Biology and Biochemistry 43 (3), 638-646. https://coi.org/https://doi.org/10.1016/j.soilbio.2010.11.035.

Temmerman, S., Meire, P., Bouma, T.J., Herman, P.M.J., Ysebaert, T., De Vriend, H.J., 2013. Ecosystem-based coastal defence in the face of global change. Nature 504 (7478), 79-83. https://coi.org/{10.1038/nature12859}.

Vasquez, E.A., Glenn, E.P., Guntenspergen, G.R., Brown, J.J., Nelson, S.G., 2006. Salt tolerance and osmotic adjustment of spartina alterniflora (poaceae) and the invasive m haplotype of phragmites australis (poaceae) along a salinity gradient. Am J Bot 93 (12), 1784-1790. https://coi.org/10.3732/ajb.93.12.1784.

Vuik, V., Jonkman, S.N., Borsje, B.W., Suzuki, T., 2016. Nature-based flood protection: the efficiency of vegetated foreshores for reducing wave loads on coastal dikes. Coast Eng 116, 42-56. https://coi.org/https://doi.org/10.1016/j.coastaleng.2016.06.001.

Vuik, V., van Vuren, S., Borsje, B.W., van Wesenbeeck, B.K., Jonkman, S.N., 2018. Assessing safety of nature-based flood defenses: dealing with extremes and uncertainties. Coast Eng 139, 47-64. https://coi.org/https://doi.org/10.1016/j.coastaleng.2018.05.002.

Wamsley, T.V., Cialone, M.A., Smith, J.M., Atkinson, J.H., Rosati, J.D., 2010. The potential of wetlands in reducing storm surge. Ocean Eng 37 (1), 59-68. https://coi.org/https://doi.org/10.1016/j.oceaneng.2009.07.018.

Wang, C., Menenti, M., Stoll, M., Belluco, E., Marani, M., 2007. Mapping mixed vegetation communities in salt marshes using airborne spectral data. Remote Sens Environ 107 (4), 559-570. https://coi.org/https://doi.org/10.1016/j.rse.2006.10.007.

Wei, W., Mei, X., Dai, Z., Tang, Z., 2016. Recent morphodynamic evolution of the largest uninhibited island in the yangtze (changjiang) estuary during 1998 – 2014: influence of the anthropogenic interference. Cont Shelf Res 124, 83-94. https://coi.org/10.1016/j.csr.2016.05.011.

Willemsen, P.W.J.M., Borsje, B.W., Vuik, V., Bouma, T.J., Hulscher, S.J.M.H., 2020. Field-based decadal wave attenuating capacity of combined tidal flats and salt marshes. Coast Eng 156, 103628. https://coi.org/https://doi.org/10.1016/j.coastaleng.2019.103628.

Yang, R., Chen, L., 2021. Spartina alterniflora invasion alters soil bulk density in coastal wetlands of china. Land Degrad Dev 32 (5), 1993-1999. https://coi.org/https://doi.org/10.1002/ldr.3859.

Yuan, J., Ding, W., Liu, D., Xiang, J., Lin, Y., 2014. Methane production potential and methanogenic archaea community dynamics along the spartina alterniflora invasion chronosequence in a coastal salt marsh. Appl Microbiol Biot 98 (4), 1817-1829. https://coi.org/10.1007/s00253-013-5104-6.

Zhang, C., Xie, Z., 2012. Combining object-based texture measures with a neural network for vegetation mapping in the everglades from hyperspectral imagery. Remote Sens Environ 124, 310-320. https://coi.org/https://doi.org/10.1016/j.rse.2012.05.015.

Zhang, M., Dai, Z., Bouma, T.J., Bricker, J., Townend, I., Wen, J., Zhao, T., Cai, H., 2021. Tidal-flat reclamation aggravates potential risk from storm impacts. Coast Eng 166, 103868. https://coi.org/https://doi.org/10.1016/j.coastaleng.2021.103868.

Zhang, M., Townend, I., Cai, H., He, J., Mei, X., 2018. The influence of seasonal climate on the morphology of the mouth-bar in the yangtze estuary, china. Cont Shelf Res 153 (Supplement C), 30-49. https://coi.org/https://doi.org/10.1016/j.csr.2017.12.004.

Zhang, M., Townend, I., Zhou, Y., Wang, L., Dai, Z., 2019. An examination of estuary stability in response to human interventions in the south branch of the yangtze (changjiang) estuary, china. Estuarine, Coastal and Shelf Science 228, 106383. https://coi.org/https://doi.org/10.1016/j.ecss.2019.106383.

Zhou, H., Liu, J., Qin, P., 2009. Impacts of an alien species (spartina alterniflora) on the macrobenthos community of jiangsu coastal inter-tidal ecosystem. Ecol Eng 35 (4), 521-528. https://coi.org/https://doi.org/10.1016/j.ecoleng.2008.06.007.